An Approach Towards Parametric Optimization of Construction Frames for Cartesian Industrial Robots

Submitted: 1st October 2021; accepted: 9th February 2022

Filip Gwardecki, Piotr Falkowski

DOI: 10.14313/JAMRIS/3-2021/15

Abstract:

The paper presents an approach to parametric optimization with response surface methodology. This process was performed based on the design of a construction frame for a Cartesian industrial robot. The presented installation is dedicated to the real industrial pick-and-place application. Firstly, the case study was described with relevant information about the components involved. Then, the finite element model with constraints and loads, as well as the settings of the response surface optimization were discussed. The simulation was presented to the reader within all the stages with necessary details. Into consideration were taken six methods of creating response surfaces. Influence on the final optimization result and prediction accuracy of each one was presented. In the end, to validate the outcomes of the process, the static structural analysis of the setup was computed. The paper compares the impact of applying different methods of response surface generation on the results of parametric optimization. Moreover, it indicates the most vulnerable fragments of dynamically loaded elements made of construction profiles. Its results may be used to select appropriate settings in similar applications, mainly for frame structures.

Keywords: *Cartesian robot, FEM, Industry 4.0, Optimization, Response surface*

1. Introduction

Over the past decades, the engineering design process has changed significantly. Computer simulations and three-dimensional modelling have been gaining more and more interest since they became commercially available. In industrial mechanical engineering, one of the most essential processes is structural analysis. It enables determining effects such as stresses, strains, and deformations of constructions caused by the loads [1]. The modern approach to solving such a problem is often based on the finite element method (FEM), which approximates a real solution [2] [3]. Considered frame structures may be discretized with one-dimensional elements with an associated specific cross-section [4] [5].

Engineers optimize their designs regarding various criteria, minimal mass among others. FEM allows tracking an impact of single structural parameters, but this approach requires many iterations carried out by a designer, to give satisfying results. Distribution and maximum value of stress depend not only on the particular cross-sections but also on the overall geometry of the structure. Moreover, the correlation between these is sometimes difficult to predict. Therefore, an effective optimization process for frames requires prior determination of all the parameters with a non-neglectable impact on the criterium. Afterwards, parametric optimization, a process of minimizing defined outputs by searching for the corresponding values of the inputs, may be carried.

It is proposed to use the response surface methodology (RSM) for optimization, so to replace the original inputs-outputs correlation model with an approximated one. This approach reduces computation time and enables the assessment of relationships between input and output parameters. However, at the same time, it reduces the precision of simulations' results. Available response surface generation algorithms are compared in terms of their approximation accuracy as well as their impact on the optimization outcomes.

The following paper aims in introducing the reader to the application of the RSM in structural design. Particularly, as more efficient use of materials is a key aspect of sustainable manufacturing and Industry 4.0.

1.1. Related Works

The RSM is widely used for the planning of chemical processes, where the course of reaction may be unknown [6] [7] [8] [9] [10]. However, the applications of this method go beyond cases where the original model is insufficiently well known. The substitute model can support the design process from an early stage by visualising the influence of design variables on key deliverables and ensuring their optimal selection [11]. The use of RSM-based adaptive models is aimed at improving accuracy [12] [13]. Whereas these generally require more computational power and are more difficult to implement, the basic RSM module is built into ANSYS Workbench 2021.

1.2. Case Description

Industrial frames are often used as support constructions for various mechanisms. In the paper, it is attached to the Cartesian manipulator presented in Fig. 1. It consists of four linear units driven by three stepper motors. Every unit converts torque from a motor into the linear force through a belt-driven mechanism. Two of them are responsible for the motion along with the same axis. This enables operation under higher loads. However, such an application requires assuring synchronous movement, realised by connecting the drives through shafts to the common engine. The robot's tasks contain transporting objects up to 100 kg from a conveyor to boxes on EUR-pallets. The

analysed frame was designed in a Computer-Aided Design (CAD) environment.

1.3. FEM and RSM

The static structural analysis of the frame was performed for the loading states resulting from the components' weights, dynamics of movements and weights of the transported objects. Dynamic reactions were traced within the multibody (MBD) analysis module during simulation operation. Their highest values, occurring while accelerating, braking, and lifting, were converted into static loads described in the next sections. Afterwards, they were applied as vertex and edge loads. Conducted analyses provide information on stress, strain and deformation distributions in a construction.

To perform optimization, selected dimensions of the frame geometry and cross-sections of the construction profiles are parametrised. Their various combinations are considered and the optimal solution is searched according to a specific criterion within the set ranges of parameters' values.

Initially, for RSM, FEM analyses are performed for the design points - sets of parameters with different values, chosen to fill the whole range of considered hyperspace. Thanks to this, an original, complex, unknown relationship between input and output parameters may be substituted with approximated hyperplanes [14]. Hence, the analytical gradients may be used for the computations to accelerate them. The estimated function is used in the optimization process providing results for applied objectives and constraints [15]. However, due to the approximation, the accuracy of the result may differ from the optimal.

Fig. 1. Visual of the Cartesian robot model

1.4. Optimization

Optimization techniques are commonly used in many different fields of science and engineering [16] [17] [18] [19] [20] [21] [22] [23]. They empower more effective usage of resources; thus cost reduction. In the paper, Multi-Objective Genetic Algorithm (MOGA) [24] [25] is used within the process of designing a supporting frame for a cartesian robot shown in Fig. 1. Optimization algorithms are continuously developed for a wide range of applications [26] [27] [28] [29] [30] [31] [32]. In general, they enable systematic search for the candidate points minimizing the loss function. In RSM, algorithms perform computations based on samples from the model. Alternatively, a direct optimization that performs calculations on the model itself, may be used. Each sample is obtained by the experiment, not a prediction in contrast to the RSM algorithms. Thus, it requires significantly more computational power but typically results in more accurate outcomes.

1.5. Considered Methods

The optimization process is based on static structural stress analysis. It is aimed at finding the most vulnerable fragments and further mass minimization with constraints involving a safety factor and total deformation. The safety factor is calculated as a ratio of the yield strength to the equivalent stress according to the Huber-Mises-Hencky hypothesis. Six methods of constructing response surfaces were taken into consideration:

1) genetic aggregation
2) full 2nd order polynomials
3) kriging
4) non-parametric regression
5) neural network
6) sparse grid

Genetic aggregation is initialized with several response surface methods with different settings. Every method has its parameters selected through genetic operations such as crossover or a mutation. Additionally, the weights for them are calculated in an analogue way; so to get the final weighted model [33].

The full second-order polynomials method approximates the real model with quadratic functions. It calculates the surfaces' parameters so as to minimize an error with respect to the real design points [34].

Kriging method obtains each surface as a combination of a global function (usually a quadratic polynomial) and local functions. The global function is determined to fit best in its whole domain, while the local functions improve accuracy only in the neighbourhood of few design points and have no effect for more distanced ones [35] [36].

Non-parametric regression comes to the use of Support Vector Machine (SVM) for regression [37]. The response surface $s(x_1, x_2, ...)$ is estimated in a way that a majority of the design points are within the e space around the surface. This space is limited with two hyperplanes, called margins and described by the minimal ϵ, as presented in Eq. 1.

$$\forall(x_1, x_2, ..., y) \in e \ : s - \epsilon \geq y \geq s + \epsilon \qquad (1)$$

Neural network estimated output parameters are calculated within a multiple-layer neural network structure. The method calculates the weights and biases so as to minimize the error between estimations and real values [38].

Sparse grid is an adaptive response surface method. It self-corrects by creating design points in the directions expected to contain inaccurate approximation. The sparse grid algorithm works well for almost all problems. It is even able to estimate a response surface with multiple discontinuities [39] [40]. However, this algorithm requires much more design points than other methods, to obtain accurate results (in this study it used around 2.5 times more points). As it requires much more computation time, it is not recommended for simpler applications.

Each of the mentioned above requires the design of the experiment phase (DoE). It is a process of defining a set of design points covering the considered ranges of input parameters. A bottleneck of the computations is calculating output parameters for these. Therefore, it is preferable to initially exclude the input parameters that have a marginal impact on the loss function in their considered ranges. For this purpose, Spearman's rank correlation matrix is being used, as it contains the linear relationship between the parameters [41]. Values close to zero indicate poor correlations and may be excluded from the optimization process.

2. Plan of the Experiment

2.1. Loads

The end effector carries an object from the conveyor to a box and then returns to its base position, over the conveyor; all during a cycle of 7.64 seconds. Within this time object needs to be gripped, transported and released. While gripping or releasing the object, the end effector should stop for 0.5 seconds. The maximum velocity is 1 m/s for the vertical linear drive and 6 m/s for the other drives. A motion along the path was planned according to all these conditions, and then, internal loads of the frame were computed with Autodesk Inventor's multi-body dynamic simulation module. The resultant forces at the three potentially most dangerous stages of motion were used afterwards for static structural analysis. These include:

1) lifting the object from the conveyor (load state 1);
2) vertical acceleration of the system after gripping the object (load state 2);
3) vertical braking of the system before releasing the object (load state 3).

Vectors of applied acceleration field, forces and torque are presented in Fig. 4. Force A (610 N) is the weight of stationary drives, while Force B (173 N) is the weight of the engine and shafts, Vector C represents earth gravity, and loads D-G are dynamic reactions of the system. Their values are gathered in Tab. 1. The frame is relatively large compared to the mounting feet, which are to be anchored. Therefore, each leg's connection to the ground is modelled as fixed support (H).

2.2. Preparation of the Model

A model of the frame in a non-native format was imported to be embedded in the Ansys SpaceClaim, where the construction profiles were replaced by beam elements. The model was parametrised with three variables represented in Fig. 2 and additionally with construction profile cross-sections' properties: thickness t and size a. Only the profile, connected with the engine and shafts, has been constrained with specific dimensions (150x140 mm). All the oblique beams were identically constrained with the same parameter describing their bases' distance from the corner of the frame. The angles between the oblique and vertical beams were taken as to 45 °. The input parameters were considered within certain scopes being a result of available space (e.g. front beam could not be placed too low, as to allow replacement of the storage boxes on pallets) and normalization standards of commercial parts. As construction profiles are available in standardized series, their typical combinations of dimensions were used. The corners of the profiles are rounded; however, for simulation purposes, they were simplified for the Ansys beam tool. The comparison of the simplified and real cross-sections is presented in Fig. 3. As proved for the initial simulation, this simplification does not significantly affect the profiles' moments of inertia and thus, calculated stresses and strains.

The frame's mesh consists of three-node one-dimensional elements of a default size of 20 mm. The element size was forced to 0.1 mm at the ends of every beam (see Fig. 5). The statistics of the mesh are presented in Tab. 3. Stainless steel (from General Materials in Ansys Workbench 2021) was assigned as the material of the construction profiles. Its strength parameters correspond to those of commonly used industrial materials. They are presented in Tab. 4 in comparison with steel used for such construction profiles. The chosen material, X5CrNiMo17-12-2, is compliant with the EN 1.4401 standard, which is the equivalent of the AISI 316 standard. [42].

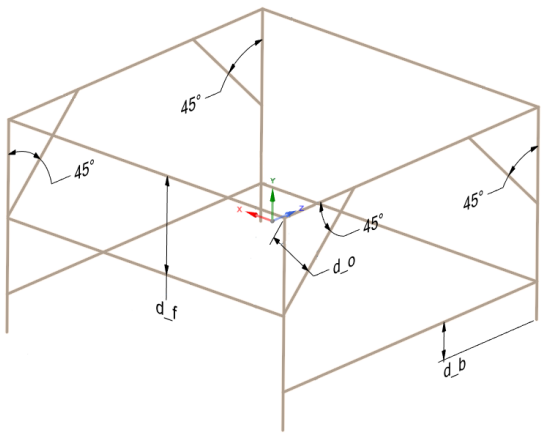

Fig. 2. Model of the frame geometry

Load State	Remote Force D [N]	Remote Force E [N]	Remote Force F [N]	Torque G [Nm]
1	0	0	3605	0
2	3448.9	0	0	26.25
3	0	3448.9	0	-26.25

Tab. 1. Values of loads

Stress distribution across beams is not constant due to the internal changes in the bending moment. Therefore, the distributions of maximum and minimum stress along a beam were analysed. Safety factor (FS) was calculated based on the calculated stress values, according to the formula Eq. 2.

$$FS = \frac{R_e}{max(|\sigma_{max}|, |\sigma_{min}|)} \tag{2}$$

Where the used symbols represent particular parameters: R_e - yield strength, σ_{max} - maximum combined stress, σ_{min} - minimum combined stress.

Geometry mass, safety factor, and maximum total deformation were set as the output parameters. FEM analysis was performed for each load state described in the previous sections. Afterwards, parameters correlation was checked with the analysis of the correlation matrix.

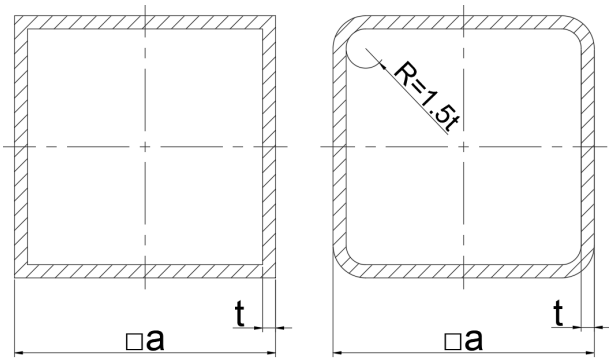

Fig. 3. Comparison of profiles' cross-sections

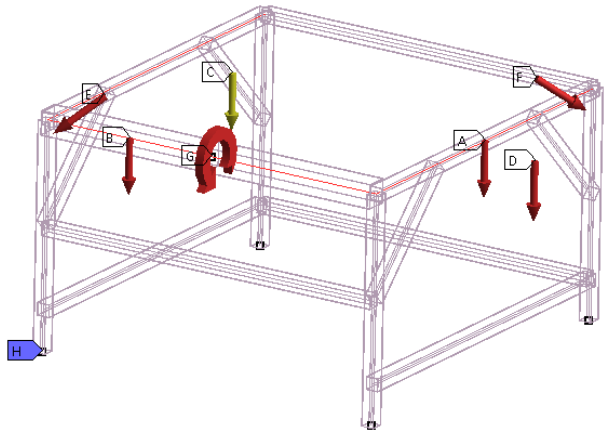

Fig. 4. Loads and boundary conditions applied to the frame

Parameter	Scope/Discrete values
d_b [mm]	$\langle 100; 400 \rangle$
d_f [mm]	$\langle 400; 700 \rangle$
d_o [mm]	$\langle 200; 820 \rangle$
a [mm]	$[60, 70, 75, 80]$
t [mm]	$[2, 3, 4]$

Tab. 2. Considered scopes for the parameters

Beams	Parametrised	Engine mounting
Elements	16368	1119
Nodes	32751	2240
Element type	Beam188	Beam188
Cross-section	a x a x t	150 x 140 x t

Tab. 3. Mesh statistics

2.3. Response Surface Optimization

Response surfaces were computed with enhanced Face-Centred Central Composite Design (FCCCD) DoE type [43] [44] (except sparse grid response surface, where the sparse grid initialization was used) and verified with 3 points not used before to create the surfaces. The DoE generally needed 53 design points, while the sparse grid generation took 131 design points. The results of optimization with the different approaches towards the generation of response surfaces were compared to choose the most suitable algorithm for similar frame constructions.

Steel	Model	EN 1.4401
Density [kg/m^3]	7750	7950
Young's Modulus [GPa]	193	200
Poisson's Ratio	0.31	0.31
Yield Strength [MPa]	207	205
Ultimate Strength [MPa]	586	515

Tab. 4. Material properties for the Ansys model and the industrial steel

Fig. 5. Frame mesh

In the end, the MOGA optimization algorithm was used for each response surface model to minimize the mass of the frame. Additionally, the safety factor was constrained to remain greater or equal to 3, while the maximum total deformation was constrained not to exceed 2 mm. The settings of the algorithm are presented in Tab. 5. Physical properties and strength results obtained with the optimal candidate points for all the methods were compared with the initial ones.

Number of initial samples	5000
Number of samples per iteration	1000
Maximum allowable pareto percentage	70
Convergance stability percentage	2
Maximum number of iterations	20
Type of discrete crossover	one point

Tab. 5. MOGA settings

3. Results

First of all, the equivalent stress analyses were conducted for the initial frame design. Their results are illustrated in terms of distribution in Fig. 6-8 with highlighted places of the maximum stresses occurring. Their values are gathered in Tab. 6.

State	σ_{max} [MPa]
Lifting	8.1634
Acceleration	17.824
Braking	18.211

Tab. 6. Maximum equivalent stress

Correlation matrix is presented in Fig. 9. The first five parameters are inputs, and the last three are outputs of optimization. The correlation coefficients between the d_f and the output parameters are almost equal to zero. Linear and quadratic trends between the d_f and the safety factor are illustrated in Fig. 10. They are used to investigate the influence of this parameter on the loss function.

Fit statistics and a response surface of safety factor as a function of d_b and d_o are presented in Fig. 11-16 for every method. The fit statistics provide accuracy

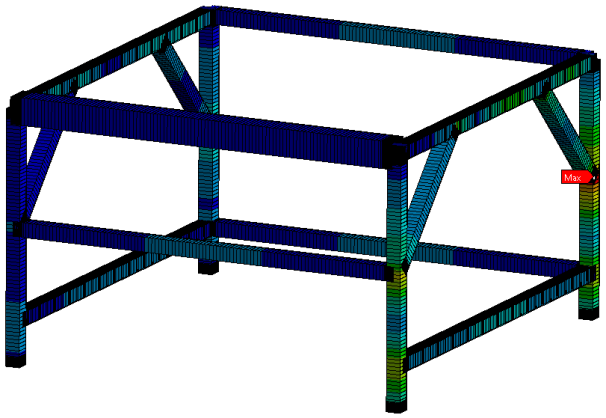

Fig. 6. Stress distribution at the load state 1

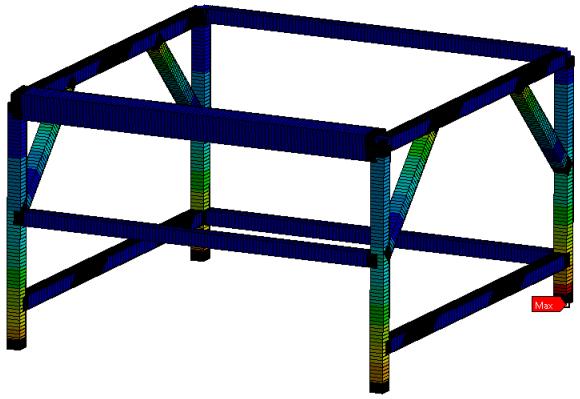

Fig. 7. Stress distribution at the load state 2

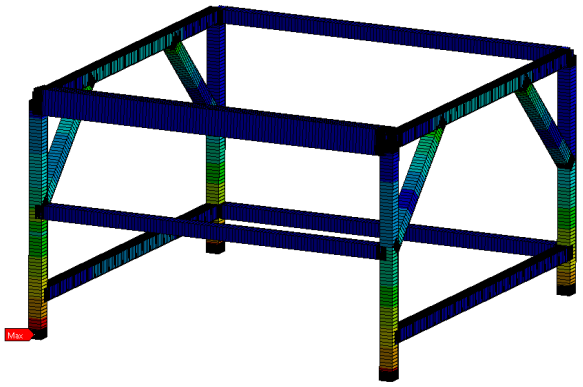

Fig. 8. Stress distribution at the load state 3

metrics of the response surface. These affect the reliability and the quality of the final results. The coefficient of determination (R^2, see Eq. 3) is a parameter that denotes how well the response surface represents the variability of the output parameter.

$$R^2 = 1 - \frac{\sum_{i=1}^{n}(y_i - \hat{y}_i)^2}{\sum_{i=1}^{n}(y_i - \bar{y})^2} \tag{3}$$

The other metrics describe errors of the approximation. These are: Root mean square error (σ, see Eq. 4);

$$\sigma = \sqrt{\frac{1}{n}\sum_{i=1}^{n}(y_i - \hat{y}_i)^2} \tag{4}$$

Relative maximum absolute error ($\sigma_{r,max}$, see Eq. 5)

$$\sigma_{r,max} = \frac{1}{\sigma} max(|y_i - \hat{y}_i|) \tag{5}$$

Relative average absolute error ($\sigma_{r,avg}$, see Eq. 6)

$$\sigma_{r,avg} = \frac{1}{n\sigma}\sum_{i=1}^{n}(|y_i - \hat{y}_i|) \tag{6}$$

The response surface function is a three-dimensional vector function of five variables. As it is impossible to represent on a single surface chart, the single response charts of one output parameter (safety factor) are presented dependent on two input parameters (d_b and d_o selected for this case, see Fig. 12-16). These specific variables were chosen due to the curvature of the surface, discussed in the following section.

The optimization results for every response surface method (named as in the first section) are compared with each other and with the ones obtained for the initial frame design (see Tab.7). Additionally, the output parameters were verified as regular design points. The safety factor and deformations were calculated for all the three load conditions. Their extreme values (minimum for safety factor and maximum for deformations) in the whole structure were used for further analysis. As may be observed, these tend to occur under load condition 3.

The figures Fig. 17-22 illustrate stress and deformation distributions for the frames optimized with every method. As may be observed, the maxima occur at approximately the same locations for every case, while the global minima are variable for stress distributions.

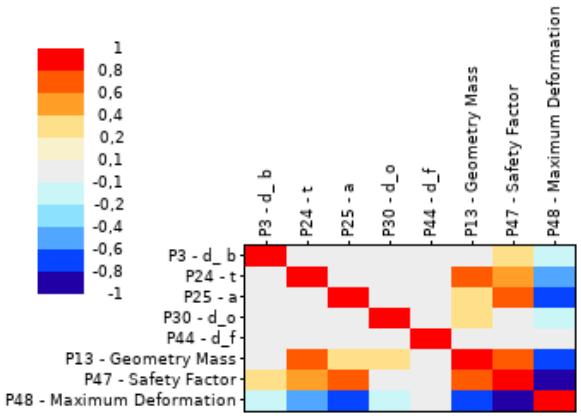

Fig. 9. Linear correlation matrix

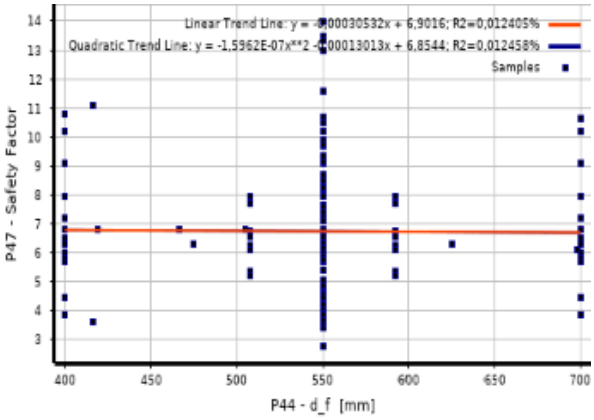

Fig. 10. Trend between the safety factor and the d_f

	P13 - Geometry Mass	P47 - Safety Factor	P48 - Maximum Total Deformation
Coefficient of Determination (Best Value = 1)			
Learning Points	1	0,99954	0,99882
Cross-Validation on Learning Points	1	0,96094	0,97256
Root Mean Square Error (Best Value = 0)			
Learning Points	0,0057286	0,064684	0,050876
Verification Points	0,026923	0,38627	0,094807
Cross-Validation on Learning Points	0,03428	0,59734	0,24575
Relative Maximum Absolute Error (Best Value = 0%)			
Learning Points	0,037419	8,3181	11,562
Verification Points	0,065882	18,532	8,3057
Cross-Validation on Learning Points	0,21887	71,687	53,482
Relative Average Absolute Error (Best Value = 0%)			
Learning Points	0	1,398	2,4264
Verification Points	0,045015	11,454	6,0593
Cross-Validation on Learning Points	0,043651	12,834	11,049

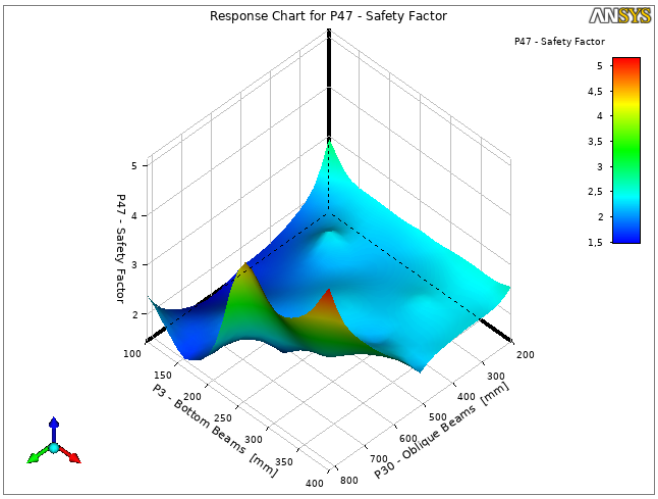

Fig. 11. The goodness of fit and the plot of response surface of safety factor dependent on d_b and d_o for genetic aggregation method

	P13 - Geometry Mass	P47 - Safety Factor	P48 - Maximum Total Deformation
Coefficient of Determination (Best Value = 1)			
Learning Points	1	0,99237	0,98838
Root Mean Square Error (Best Value = 0)			
Learning Points	0,079188	0,22358	0,142
Verification Points	2,2039	0,65901	0,28131
Relative Maximum Absolute Error (Best Value = 0%)			
Learning Points	0,34742	31,684	32,28
Verification Points	4,8972	35,677	35,551
Relative Average Absolute Error (Best Value = 0%)			
Learning Points	0,12301	5,558	7,3207
Verification Points	4,8241	24,631	16,444

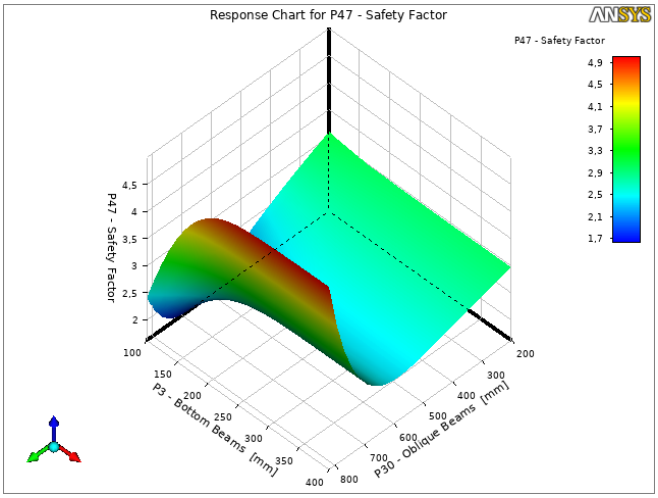

Fig. 12. The goodness of fit and the plot of response surface of safety factor dependent on d_b and d_o for second order polynomials method

	P13 - Geometry Mass	P47 - Safety Factor	P48 - Maximum Total Deformation
Coefficient of Determination (Best Value = 1)			
Learning Points	1	1	1
Root Mean Square Error (Best Value = 0)			
Learning Points	2,8115E-06	2,6686E-05	1,0622E-06
Verification Points	0,039155	0,30106	0,27149
Relative Maximum Absolute Error (Best Value = 0%)			
Learning Points	0	0	0
Verification Points	0,089589	10,694	23,038
Relative Average Absolute Error (Best Value = 0%)			
Learning Points	0	0	0
Verification Points	0,064265	9,1624	14,338

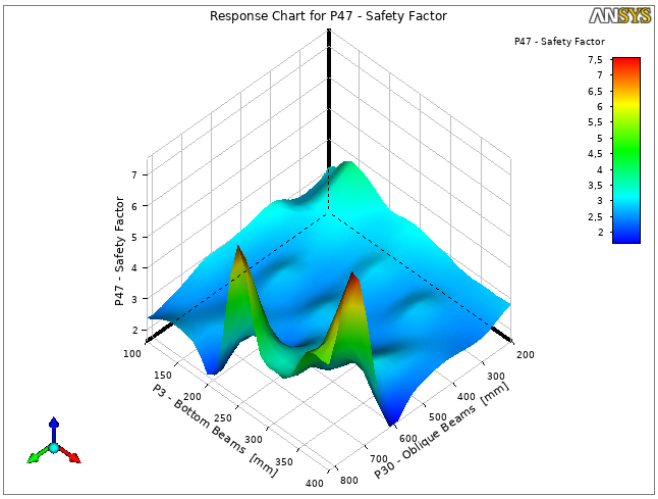

Fig. 13. The goodness of fit and the plot of response surface of safety factor dependent on d_b and d_o for kriging method

	P13 - Geometry Mass	P47 - Safety Factor	P48 - Maximum Total Deformation
Coefficient of Determination (Best Value = 1)			
Learning Points	0,99838	0,99593	0,99761
Root Mean Square Error (Best Value = 0)			
Learning Points	1,8176	0,16328	0,06439
Verification Points	27,549	1,2443	0,7675
Relative Maximum Absolute Error (Best Value = 0%)			
Learning Points	4,7891	23,963	5,735
Verification Points	95,574	61,524	80,03
Relative Average Absolute Error (Best Value = 0%)			
Learning Points	3,6314	5,6216	4,6513
Verification Points	51,008	46,936	52,879

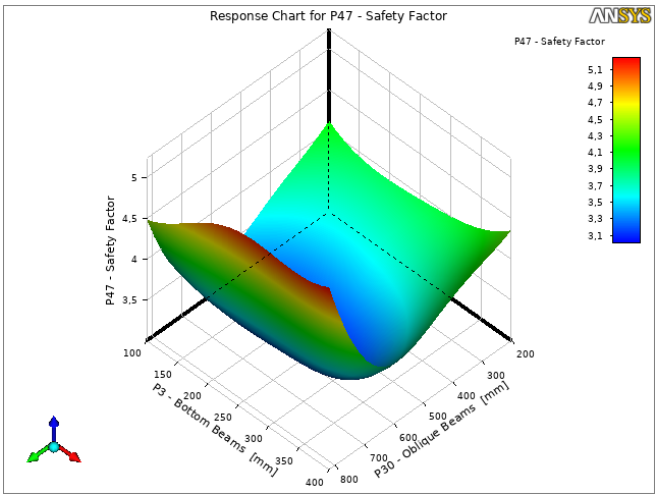

Fig. 14. The goodness of fit and the plot of response surface of safety factor dependent on d_b and d_o for non-parametric regression method

	P13 - Geometry Mass	P47 - Safety Factor	P48 - Maximum Total Deformation
Coefficient of Determination (Best Value = 1)			
Learning Points	0,98173	0,79495	0,8736
Root Mean Square Error (Best Value = 0)			
Learning Points	6,1131	1,1592	0,46841
Verification Points	12,075	1,9484	0,64881
Relative Maximum Absolute Error (Best Value = 0%)			
Learning Points	68,878	190,25	172,98
Verification Points	41,567	117,03	58,083
Relative Average Absolute Error (Best Value = 0%)			
Learning Points	5,0829	29,869	17,268
Verification Points	20,555	66,126	48,41

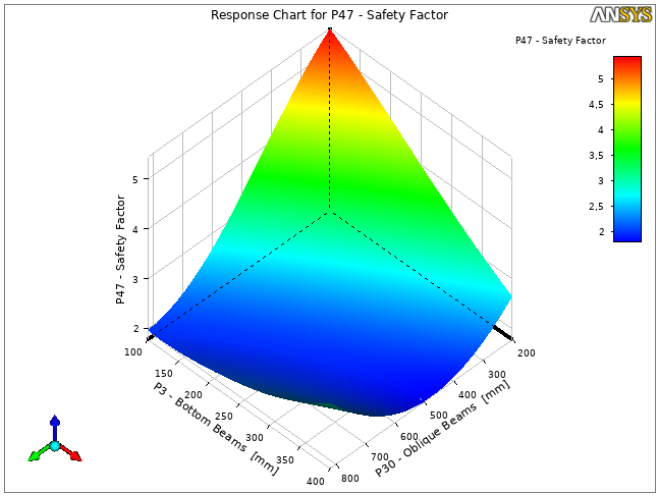

Fig. 15. The goodness of fit and the plot of response surface of safety factor dependent on d_b and d_o for neural network method

	P13 - Geometry Mass	P47 - Safety Factor	P48 - Maximum Total Deformation
Coefficient of Determination (Best Value = 1)			
Learning Points	1	1	1
Root Mean Square Error (Best Value = 0)			
Learning Points	0	0	0
Verification Points	0,70684	0,021004	0,077043
Relative Maximum Absolute Error (Best Value = 0%)			
Learning Points	0	0	0
Verification Points	2,0178	1,055	12,227
Relative Average Absolute Error (Best Value = 0%)			
Learning Points	0	0	0
Verification Points	1,8526	0,93214	4,4928

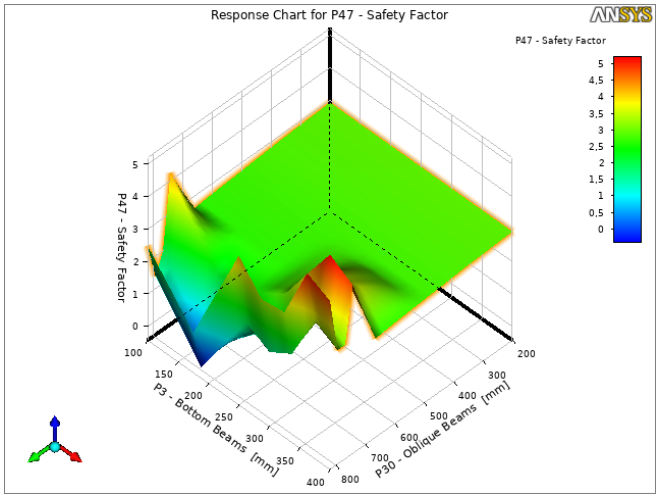

Fig. 16. The goodness of fit and the plot of response surface of safety factor dependent on d_b and d_o for sparse grid method

Method (number)	1	2	3	4	5	6	Initial Frame
d_b [mm]	179.69	364.25	113.33	120.67	298.31	130.04	200.00
d_f [mm]	429.75	456.55	409.66	417.48	662.74	419.34	600.00
d_o [mm]	200.43	203.82	256.25	203.61	200.64	200.20	450.00
Profile size [mm]	80	80	75	75	75	80	80
Profile thickness [mm]	2	2	2	2	2	2	4
Geometry mass [kg]	131.94	130.39	126.91	131.71	125.25	130.79	-
Safety factor	6.9842	6.6271	5.7762	6.6254	6.7461	6.8452	-
Maximum deformation [mm]	1.7331	1.9063	1.9924	1.9664	1.9981	1.7334	-
Geometry mass (verified) [kg]	131.95	132.06	126.79	124.88	124.77	131.95	276.42
Safety factor (verified)	6.7984	6.7957	6.0372	6.0982	6.1023	6.7981	11.367
Maximum deformation (verified)[mm]	1.7812	1.7814	2.0904	2.0906	2.0861	1.7798	0.8722

Tab. 7. Optimization results for different methods

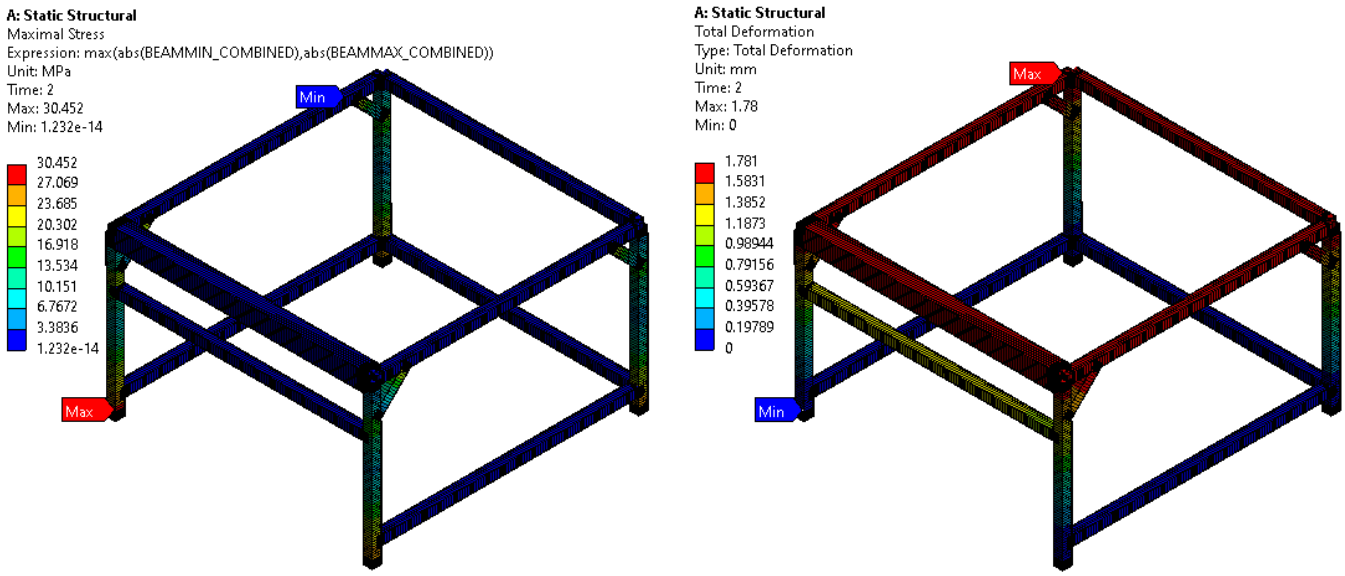

Fig. 17. The equivalent stress distribution and the deformation at the load state 3 for genetic aggregation configuration

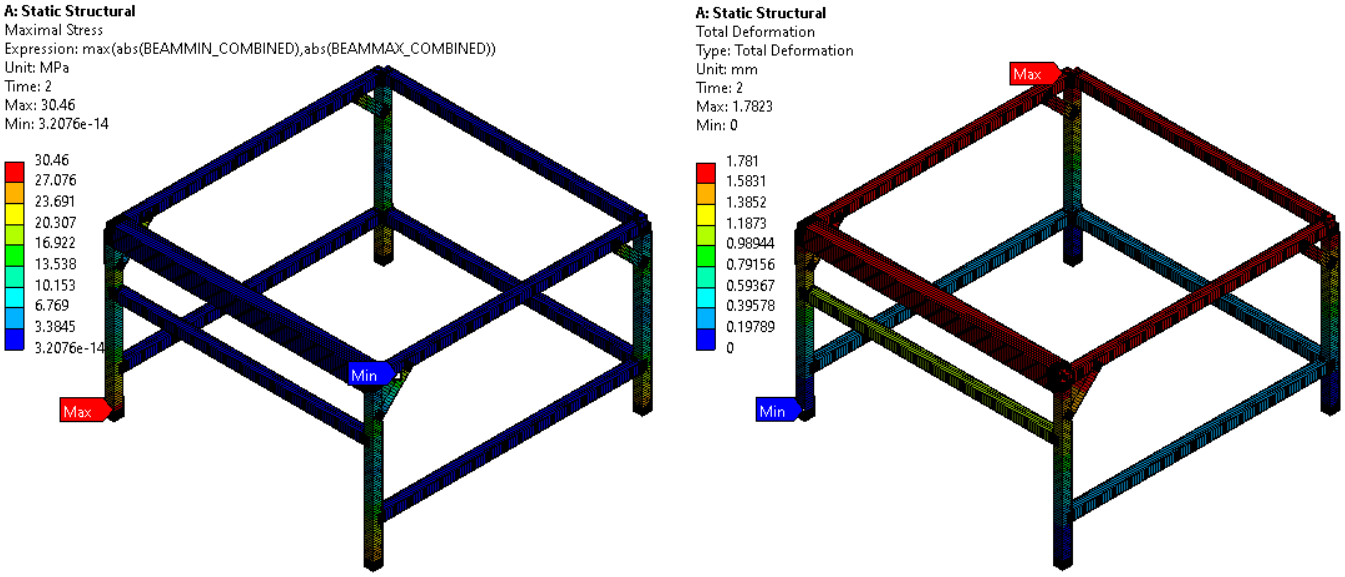

Fig. 18. The equivalent stress distribution and the deformation at the load state 3 for 2nd order polynomials configuration

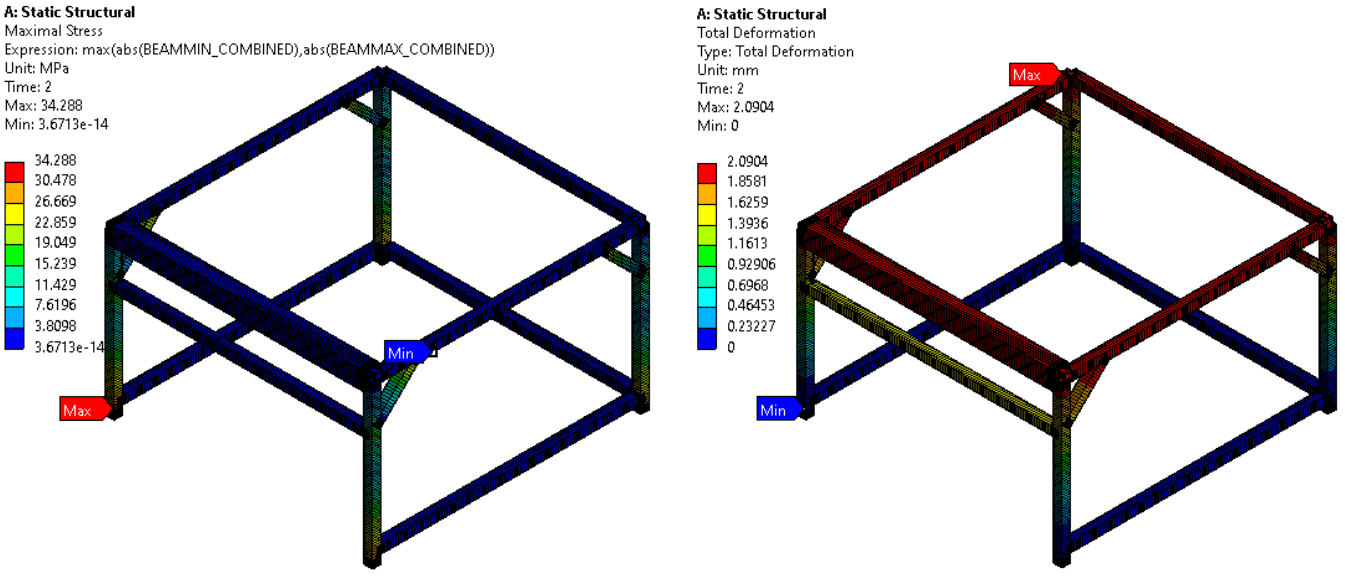

Fig. 19. The equivalent stress distribution and the deformation at the load state 3 for kriging configuration

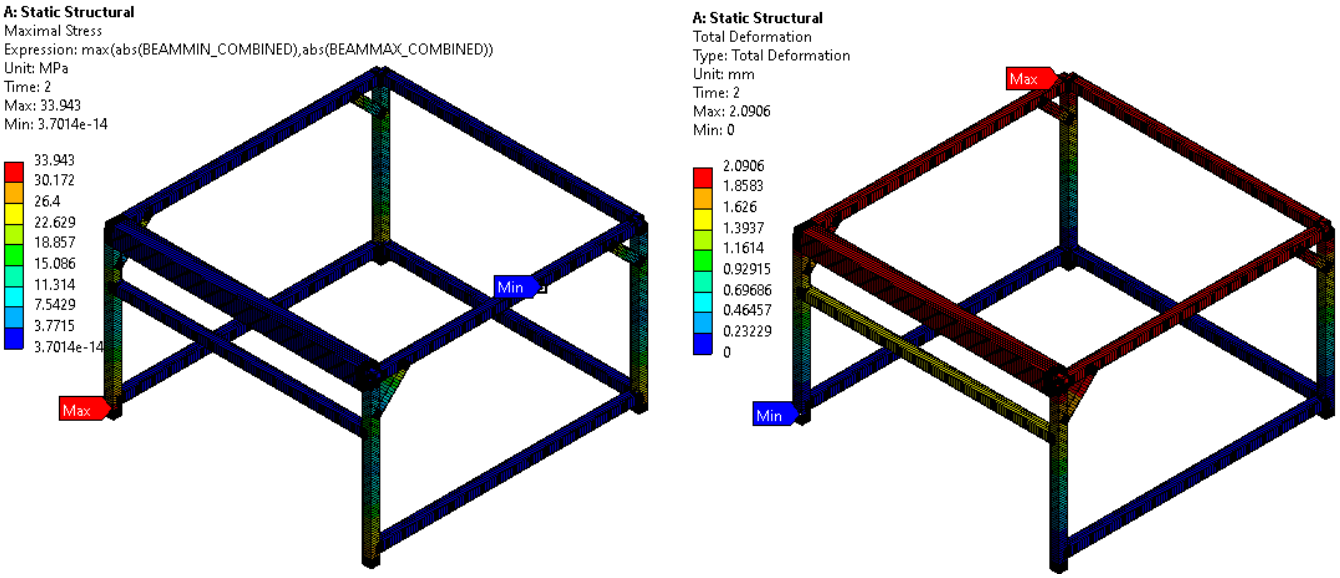

Fig. 20. The equivalent stress distribution and the deformation at the load state 3 for non-parametric regression configuration

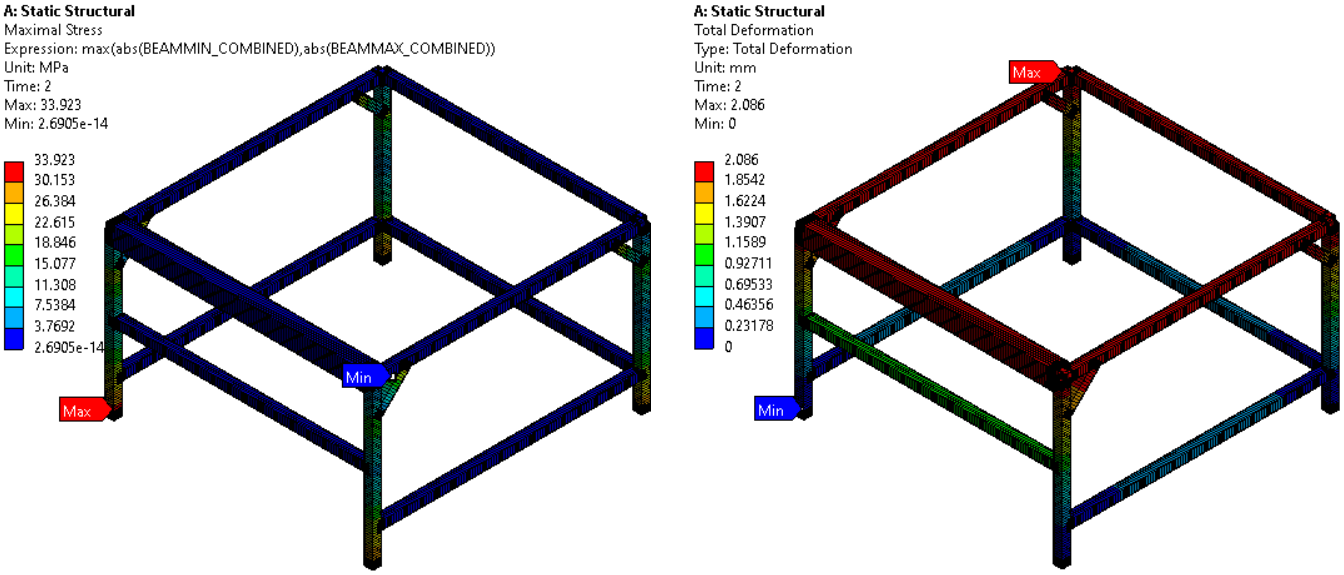

Fig. 21. The equivalent stress distribution and the deformation at the load state 3 for neural network configuration

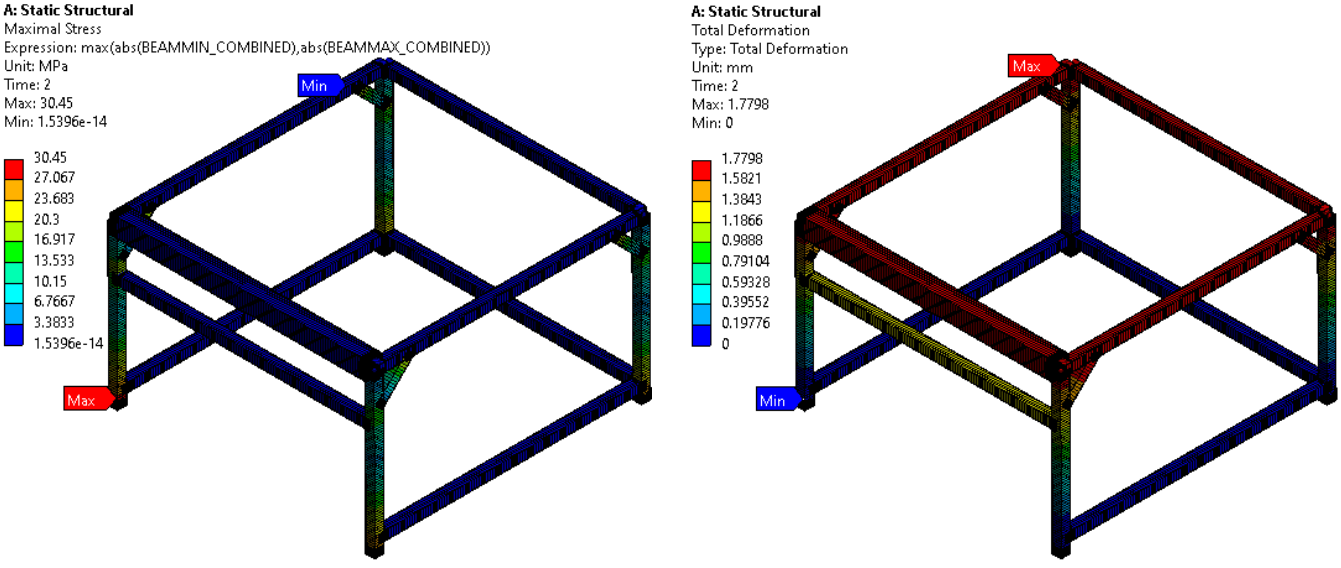

Fig. 22. The equivalent stress distribution and the deformation at the load state 3 for sparse grid configuration

4. Discussion of the Results

According to the FEM analysis of the frame, the parts connected to the ground are the ones with the highest values of internal stress. They are especially exposed to damage within load cases 1 and 3. It is the result of the greatest local internal torque caused by the horizontal component of the dynamic response. Regarding this, frame structures are typically more loaded during acceleration and deceleration of the Cartesian robot's horizontal units. Moreover, the surrounding of the load application point is more stressed than the other fragments of the frame. As the design is overly stiff, the entire load is distributed among the supports. Such a dependence shall occur for the frame parts connecting the force application points with the constraint points for the constructions with similar stiffness properties. The longer the beam, the more flexible it is, and thus, transfers less load to the support.

The correlation coefficients of the d_f with the outputs indicate that this parameter has almost no influence on the loss function within the considered scope. Also, an analysis of the linear and quadratic trend graphs confirm this theory. Therefore, it could have been excluded from the optimization process. As expected, the response surfaces involving this parameter indicated almost no relationship with outputs.

Regarding different methods of response surface generation, the sparse grid obtained the best metrics of quality. Genetic aggregation and kriging methods estimated geometry mass correctly. However, their stress and deformation estimations remained less accurate. The second-order polynomials algorithm provided decent geometry mass estimations but failed in determining stress and deformation responses. Finally, non-parametric regression and the approach based on neural networks provided the worst fitting response surfaces.

The included charts of safety factors may be used to define the cause of the insufficient fit for response surface models. As observed, the stress changes rapidly for the upper range of input parameters associated with oblique beams. The tendency is similar for the correlation between these parameters and the total deformation.

The kriging and genetic aggregation algorithms provide wavy response surfaces, while others, except the sparse grid, provide smooth ones. The response surface for the sparse grid algorithm is irregular with a sharp geometry. It is especially visible for the higher values of the parameter related to oblique beams and the extremal values of the parameter related to the bottom beams. This can be observed in Fig. 12-16, as well as for other response surfaces not presented in this paper.

Genetic aggregation and kriging provide acceptable metrics for learning points. However, the verifications points indicate that the response surface models are less accurate. This situation may be caused by a lack of design points especially for such a high variability of the safety factor.

The second-order polynomials method resulted in poor metrics for the safety factor and deformation estimations. This means that quadratic functions are insufficient to estimate curvatures of the real responses. Similar outcomes may be observed for non-parametric regression and neural networks approach.

Even though some algorithms had poor quality metrics, all methods provided similar results of optimization. Some of them underestimated displacement and while verifying, it turned out to exceed the boundary limit. However, as the RSM is a numerical estimation, some minor inaccuracies should be considered and acceptable. The genetic aggregation involves significantly fewer points and leads to almost the same outcomes as the sparse grid, for relatively simple construction of a frame. Therefore, it is not recommended to use such a complex method if there are no extraordinary circumstances, such as expected discontinuities in the inputs-outputs function.

The stress distributions in the optimized structures are similar to those for the initial design under the same loading condition. Also, the maxima for both, stress and deformation, occur at the same locations for all the methods.

5. Conclusion

The rising importance of digital technologies and particular simulations in the design process brings new possibilities for engineers. This arises a need to understand the basics of numerical algorithms laying behind these. Related knowledge and experience are useful to select appropriate methods from their wide range. This is especially important for FEM, as the decision on modelling the system and setting the computations may significantly affect their results.

In frame structures, it is advisable to inspect the connections and joints in the nearby surroundings of the frame-ground interface. This is necessary due to the higher values of the stress appearing there. All the simulations shall be run for the extremal load cases, hence, for the greatest moment occurring nearby the supports.

Response surface optimization is a powerful tool to reduce mass at the early stage of design. Additionally, dependencies between input and output parameters may be analysed by the engineer to empower suboptimal manual design. Within response surface optimization, the key aspect is to select an adequate method for an expected characteristic of the response. However, this may be difficult for multi-output systems with numerous variables. The previous sections may be used as a base for the optimization of similar frame constructions. Nevertheless, the quality metrics of the models obtained with a particular method shall be controlled at all stages. The amount of necessary design points increases with the number of input parameters, the span of their ranges and the complexity of the response. However, it depends mainly on the number of variables, as the domain of the estimated response grows linearly with the number of their combinations.

All the considered methods provided appropriate optimization results. However, genetic aggregation, kriging and the sparse grid had noticeably better accuracy metrics. These methods are expected to give correct results for similar frame constructions; i.e. a frame on a rectangular plan without a base and with additional diagonal reinforcing beams fixed in the corners, particularly for the similar cross-sections and overall dimensions.

The wavy response surfaces cause a better local fit of kriging, genetic aggregation and sparse grid methods to the design points. Therefore, they are better suited for nonlinear and dynamically changing responses. However, they are less effective if the data is noisy, e.g. for the sets with a measurement error.

The investigation may be continued in three different directions. First of all, it is possible to test the application of RSM for more complex frames as well as the structures with two- and three-dimensional finite elements. The results of such an experiment should enable forming a benchmark of geometries connected with the best-fitted RSM methods. Second of all, it is possible to perform direct optimization and compare the accuracy gain, considering the additional computational cost. Also, the use of adaptive models for the design of similar industrial frames can be tested. The original research is planned to be followed up within the first approach, and possibly broadened for a variety of materials as well as manufacturing techniques.

AUTHORS

Filip Gwardecki* – Warsaw University of Technology, Plac Politechniki 1, Warsaw, 00-661, e-mail: filip.gwardecki.stud@pw.edu.pl.

Piotr Falkowski* – ŁUKASIEWICZ Research Network – Industrial Research Institute for Automation and Measurements PIAP, Al. Jerozolimskie 202, Warsaw, Warsaw University of Technology, 02-486, Plac Politechniki 1, Warsaw, 00-661, e-mail: piotr.falkowski@piap.lukasiewicz.gov.pl.

*Corresponding author

REFERENCES

[1] T. H. G. Megson, *Structural and stress analysis*, Butterworth-Heinemann, an imprint of Elsevier: Kidlington, Oxford Cambridge, MA, 2019.

[2] D. G. Pavlou. "Chapter 2 - Mathematical Background". In: D. G. Pavlou, ed., *Essentials of the Finite Element Method*, 19–40. Academic Press, January 2015. 10.1016/B978-0-12-802386-0.00002-5.

[3] P. Falkowski, B. Wittels, Z. Pilat, and M. Smater, "Capabilities of the Additive Manufacturing in Rapid Prototyping of the Grippers' Precision Jaws". In: R. Szewczyk, C. Zieliński, and M. Kaliczyńska, eds., *Automation 2019*, Cham, 2020, 379–387, 10.1007/978-3-030-13273-6_36.

[4] D. G. Pavlou. "Chapter 6 - Beams". In: D. G. Pavlou, ed., *Essentials of the Finite Element Method*, 135–212. Academic Press, January 2015. 10.1016/B978-0-12-802386-0.00006-2.

[5] D. G. Pavlou. "Chapter 7 - Frames". In: D. G. Pavlou, ed., *Essentials of the Finite Element Method*, 213–278. Academic Press, January 2015. 10.1016/B978-0-12-802386-0.00007-4.

[6] L. M. S. Pereira, T. M. Milan, and D. R. Tapia-Blácido, "Using Response Surface Methodology (RSM) to optimize 2G bioethanol production: A review", *Biomass and Bioenergy*, vol. 151, 2021, 106166, 10.1016/j.biombioe.2021.106166.

[7] J. R. Hanumanthu, G. Ravindiran, R. Subramanian, and P. Saravanan, "Optimization of process conditions using RSM and ANFIS for the removal of Remazol Brilliant Orange 3R in a packed bed column", *Journal of the Indian Chemical Society*, vol. 98, no. 6, 2021, 100086, 10.1016/j.jics.2021.100086.

[8] C. V. Rekhate and J. K. Srivastava, "Effectiveness of O3/Fe2+/H2O2 process for detoxification of heavy metals in municipal wastewater by using RSM", *Chemical Engineering and Processing - Process Intensification*, vol. 165, 2021, 108442, 10.1016/j.cep.2021.108442.

[9] H. Masoumi, A. Ghaemi, and H. Gilani Ghanadzadeh, "Elimination of lead from multicomponent lead-nickel-cadmium solution using hyper-cross-linked polystyrene: Experimental and RSM modeling", *Journal of Environmental Chemical Engineering*, vol. 9, no. 6, 2021, 106579, 10.1016/j.jece.2021.106579.

[10] N. Gammoudi, M. Mabrouk, T. Bouhemda, K. Nagaz, and A. Ferchichi, "Modeling and optimization of capsaicin extraction from Capsicum annuum L. using response surface methodology (RSM), artificial neural network (ANN), and Simulink simulation", *Industrial Crops and Products*, vol. 171, 2021, 113869, 10.1016/j.indcrop.2021.113869.

[11] V. Cipolla, K. Abu Salem, G. Palaia, V. Binante, and D. Zanetti, "A DoE-based approach for the implementation of structural surrogate models in the early stage design of box-wing aircraft", *Aerospace Science and Technology*, vol. 117, 2021, 106968, 10.1016/j.ast.2021.106968.

[12] D. Meng, Y. Li, C. He, J. Guo, Z. Lv, and P. Wu, "Multidisciplinary design for structural integrity using a collaborative optimization method based on adaptive surrogate modelling", *Materials & Design*, vol. 206, 2021, 109789, 10.1016/j.matdes.2021.109789.

[13] H. Xu, L. Liu, and M. Zhang, "Adaptive surrogate model-based optimization framework applied to battery pack design", *Materials & Design*, vol. 195, 2020, 108938, 10.1016/j.matdes.2020.108938.

[14] S. K. Behera, H. Meena, S. Chakraborty, and B. C. Meikap, "Application of response surface methodology (RSM) for optimization of leaching

parameters for ash reduction from low-grade coal", *International Journal of Mining Science and Technology*, vol. 28, no. 4, 2018, 621–629, 10.1016/j.ijmst.2018.04.014.

[15] A. Menon. "Structural Optimization Using ANSYS and Regulated Multiquadric Response Surface Model", 2005. MS Thesis.

[16] C. Juarez-Santini, M. Ornelas-Rodriguez, J. A. Soria-Alcaraz, A. Rojas-Domínguez, H. J. Puga-Soberanes, A. Espinal, and H. Rostro-Gonzalez, "Single Spiking Neuron Multi-Objective Optimization for Pattern Classification", *Journal of Automation, Mobile Robotics and Intelligent Systems*, vol. 14, no. 1, 2020, 73–80, 10.14313/JAMRIS/1-2020/9.

[17] Y. Poma, P. Melin, C. I. González, and G. E. Martínez, "Optimization of Convolutional Neural Networks Using the Fuzzy Gravitational Search Algorithm", *Journal of Automation, Mobile Robotics and Intelligent Systems*, vol. 14, no. 1, 2020, 109–120, 10.14313/JAMRIS/1-2020/12.

[18] L. Daniyan, E. Nwachukwu, I. Daniyan, and O. Bonaventure, "Development and Optimization of an Automated Irrigation System", *Journal of Automation, Mobile Robotics and Intelligent Systems*, vol. 13, no. 1, 2019, 37–45, 10.14313/JAMRIS_1-2019/5.

[19] S. Patel, D. Israni, and P. Shah, "Path Planning Optimization and Object Placement Through Visual Servoing Technique for Robotics Application", *Journal of Automation, Mobile Robotics and Intelligent Systems*, vol. 14, no. 1, 2020, 39–47, 10.14313/JAMRIS/1-2020/5.

[20] S.-P. Zhu, B. Keshtegar, N.-T. Trung, Z. M. Yaseen, and D. T. Bui, "Reliability-based structural design optimization: hybridized conjugate mean value approach", *Engineering with Computers*, vol. 37, no. 1, 2021, 381–394, 10.1007/s00366-019-00829-7.

[21] J. Yan, O. A. Broesicke, X. Tong, D. Wang, D. Li, and J. C. Crittenden, "Multidisciplinary design optimization of distributed energy generation systems: The trade-offs between life cycle environmental and economic impacts", *Applied Energy*, vol. 284, 2021, 116197, 10.1016/j.apenergy.2020.116197.

[22] H. Shi, Y. Gao, and X. Wang, "Optimization of injection molding process parameters using integrated artificial neural network model and expected improvement function method", *The International Journal of Advanced Manufacturing Technology*, vol. 48, no. 9, 2010, 955–962, 10.1007/s00170-009-2346-7.

[23] X. Liu, X. Liu, Z. Zhou, and L. Hu, "An efficient multi-objective optimization method based on the adaptive approximation model of the radial basis function", *Structural and Multidisciplinary Optimization*, vol. 63, no. 3, 2021, 1385–1403, 10.1007/s00158-020-02766-2.

[24] N. A. Zolpakar, S. S. Lodhi, S. Pathak, and M. A. Sharma. "Application of Multi-objective Genetic Algorithm (MOGA) Optimization in Machining Processes". In: K. Gupta and M. K. Gupta, eds., *Optimization of Manufacturing Processes*, Springer Series in Advanced Manufacturing, 185–199. Springer International Publishing, Cham, 2020.

[25] C. Liu, W. Bu, and D. Xu, "Multi-objective shape optimization of a plate-fin heat exchanger using CFD and multi-objective genetic algorithm", *International Journal of Heat and Mass Transfer*, vol. 111, 2017, 65–82, 10.1016/j.ijheatmasstransfer.2017.03.066.

[26] K. Lenin, "Active Power Loss Reduction by Novel Feral Cat Swarm Optimization Algorithm", *Journal of Automation, Mobile Robotics and Intelligent Systems*, vol. 14, no. 2, 2020, 25–29, 10.14313/JAMRIS/2-2020/16.

[27] K. Lenin, "A Novel Merchant Optimization Algorithm for Solving Optimal Reactive Power Problem", *Journal of Automation, Mobile Robotics and Intelligent Systems*, vol. 15, no. 1, 2021, 51–56, 10.14313/JAMRIS/1-2021/7.

[28] F. Valdez, Y. Kawano, and P. Melin, "Toward the Best Combination of Optimization with Fuzzy Systems to Obtain the Best Solution for the GA and PSO Algorithms Using Parallel Processing", *Journal of Automation, Mobile Robotics and Intelligent Systems*, vol. 14, no. 1, 2020, 55–64, 10.14313/JAMRIS/1-2020/7.

[29] A. Santiago, B. Dorronsoro, A. J. Nebro, J. J. Durillo, O. Castillo, and H. J. Fraire, "A novel multi-objective evolutionary algorithm with fuzzy logic based adaptive selection of operators: FAME", *Information Sciences*, vol. 471, 2019, 233–251, 10.1016/j.ins.2018.09.005.

[30] F. Olivas, F. Valdez, P. Melin, A. Sombra, and O. Castillo, "Interval type-2 fuzzy logic for dynamic parameter adaptation in a modified gravitational search algorithm", *Information Sciences*, vol. 476, 2019, 159–175, 10.1016/j.ins.2018.10.025.

[31] E. Bernal, M. L. Lagunes, O. Castillo, J. Soria, and F. Valdez, "Optimization of Type-2 Fuzzy Logic Controller Design Using the GSO and FA Algorithms", *International Journal of Fuzzy Systems*, vol. 23, no. 1, 2021, 42–57, 10.1007/s40815-020-00976-w.

[32] G. Eichfelder, "Twenty years of continuous multiobjective optimization in the twenty-first century", *EURO Journal on Computational Optimization*, vol. 9, 2021, 100014, 10.1016/j.ejco.2021.100014.

[33] S. Wang, G. Jian, J. Xiao, J. Wen, and Z. Zhang, "Optimization investigation on configuration parameters of spiral-wound heat exchanger using Genetic Aggregation response surface and Multi-Objective Genetic Algorithm", *Applied*

Thermal Engineering, vol. 119, 2017, 603–609, 10.1016/j.applthermaleng.2017.03.100.

[34] N. Hao, Y. Feng, and H. H. Zhang, "Model Selection for High-Dimensional Quadratic Regression via Regularization", *Journal of the American Statistical Association*, vol. 113, no. 522, 2018, 615–625, 10.1080/01621459.2016.1264956.

[35] C. F. J. Wu and M. Hamada. "Computer Experiments". In: *Experiments: Planning, Analysis, and Optimization*, Wiley Series in Probability and Statistics. Wiley, 3rd edition, February 2021.

[36] J. Zeng, Z.-H. Tan, T. Matsunaga, and T. Shirai, "Generalization of Parameter Selection of SVM and LS-SVM for Regression", *Machine Learning and Knowledge Extraction*, vol. 1, no. 2, 2019, 745–755, 10.3390/make1020043.

[37] M. Nouioua, M. A. Yallese, R. Khettabi, S. Belhadi, M. L. Bouhalais, and F. Girardin, "Investigation of the performance of the MQL, dry, and wet turning by response surface methodology (RSM) and artificial neural network (ANN)", *The International Journal of Advanced Manufacturing Technology*, vol. 93, no. 5, 2017, 2485–2504, 10.1007/s00170-017-0589-2.

[38] J. Garcke. "Sparse Grids in a Nutshell". In: J. Garcke and M. Griebel, eds., *Sparse Grids and Applications*, volume 88, 57–80. Springer Berlin Heidelberg, Berlin, Heidelberg, 2012.

[39] G. Zhang, C. Webster, M. Gunzburger, and J. Burkardt, "A Hyperspherical Adaptive Sparse-Grid Method for High-Dimensional Discontinuity Detection", *SIAM Journal on Numerical Analysis*, vol. 53, no. 3, 2015, 1508–1536.

[40] T. S. Ramu. "6.19.1 Correlation Coefficient". In: *Diagnostic Testing and Life Estimation of Power Equipment*. New Academic Science, Kent, 2009.

[41] P. D. Harvey. "4.17.3 Physical Properties". In: P. D. Harvey, ed., *Engineering properties of steel*. American Society for Metals, Metals Park, Ohio, 1982.

[42] T. N. Nguyen, *Materials and Processing Technologies*, Trans Tech Publications, Limited: Zurich, 2020.

[43] C. F. J. Wu and M. Hamada. "Response Surface Methodology". In: *Experiments: Planning, Analysis, and Optimization*, Wiley Series in Probability and Statistics. Wiley, 3 edition, February 2021.